International Journal of Multidisciplinary Studies and Innovative Technologies

e-ISSN: 2602-4888
dergipark.org.tr/en/pub/ijmsit
Research Article

2026, 10 (1), 9-22
DOI: 10.36287/ijmsit.10.1.2
Received: April 8, 2026; Accepted: May 31, 2026

Adaptive Control-Based Reconfigurable Boost Converter Architecture for Photovoltaic Power Conversion Under Variable Conditions

Burak Kara [1*], Cem Emeksiz[2] and Mehmet Serhat Can[3]

[1*] *Tokat Vocational High School, Tokat Gaziosmanpasa University, Tokat, Türkiye (burak.kara@gop.edu.tr) (ORCID: 0000-0002-4453-6515)*

[2] *Department of Electrical and Electronics Engineering, Tokat Gaziosmanpasa University, Tokat, Türkiye (cem.emeksiz@gop.edu.tr) (ORCID: 0000-0002-4817-9607)*

[3] *Department of Electrical and Electronics Engineering, Tokat Gaziosmanpasa University, Tokat, Türkiye (mehmetserhat.can@gop.edu.tr) (ORCID: 0000-0003-2356-9921)*

Abstract – This study proposes a time-dependent switched adaptive boost converter architecture to enhance dynamic stability and improve power transfer efficiency in photovoltaic (PV) systems operating under varying irradiance and temperature conditions. Conventional boost converters typically use fixed passive components, which often lead to overshoot, oscillations, and instability during rapid environmental changes. These issues negatively impact both converter performance and the effectiveness of maximum power point tracking (MPPT) algorithms. In the proposed approach, groups of inductors and capacitors are dynamically switched on and off through a time-based control mechanism, allowing real-time reconfiguration of the converter topology. This adaptive configuration introduces an additional energy buffering capability, thereby improving the system's transient response against sudden irradiance fluctuations. The system was modeled and simulated in the MATLAB Simulink environment and evaluated using Perturb and Observe (P&O), Incremental Conductance (IC), and a hybrid Particle Swarm Optimization–Incremental Conductance (PSO–IC) MPPT algorithms. Comparative results between classical and adaptive converter structures demonstrate that the proposed system achieves lower root mean square error (RMSE), reduced mean absolute percentage error (MAPE), and decreased output power ripple. Among the tested methods, the adaptive converter integrated with the PSO–IC hybrid algorithm exhibited the best performance, achieving a tracking efficiency of 96.56%, faster convergence, and minimized power oscillations. Overall, the proposed adaptive converter structure provides a more stable, accurate, and efficient energy conversion compared to traditional designs, significantly enhancing the reliability of PV systems and MPPT performance. Future work will focus on hardware implementation and evaluation with alternative metaheuristic MPPT techniques.

Keywords *– Photovoltaic system, Adaptive boost converter, MPPT, PSO-IC algorithm, MATLAB/Simulink*

Citation: Kara, B., Emeksiz, C., Can, M.S. (2026). Adaptive Control-Based Reconfigurable Boost Converter Architecture for Photovoltaic Power Conversion Under Variable Conditions. International Journal of Multidisciplinary Studies and Innovative Technologies, 10(1): 9-22.

I. Introduction

Energy demand is increasing day by day due to technological developments and population growth. Due to the limited supply of fossil fuels and the negative environmental impacts they cause, countries around the world are turning to alternative energy sources. Renewable energy sources are preferred as alternatives because they are environmentally friendly and do not cause harmful waste. As of July 2025, the total installed electricity capacity in our country has reached 119,632 MW. The distribution of installed capacity by source is as follows: 27% from hydroelectric energy, 20.6% from natural gas, 18.3% from coal, 11.3% from wind, 19.2% from solar, 1.4% from geothermal, and 2.2% from other sources [1].

Among renewable energy sources, the most preferred are solar energy, wind energy, and hydroelectric energy. Among these renewable energy sources, solar energy is at the forefront of energy sources whose popularity is increasing day by day [2], [3]. Solar power plants have advantages such as being environmentally friendly, having low installation costs, and not requiring frequent maintenance [2], [4], [5]. For solar energy systems to be used efficiently, they must operate at maximum power point. Tracking systems (single-axis, dual-axis) and the control algorithms used in these systems are required to track the maximum power point [2], [6]. This is because the panel's maximum power point constantly changes due to varying solar radiation intensities and temperature values. Among the most commonly used maximum power point tracking (MPPT) algorithms in maximum power tracking systems are the Perturb & Observe and incremental conductance algorithms. These algorithms are frequently preferred due to their simplicity and low computational load. Artificial neural networks, particle swarm optimization, gray wolf optimization, genetic algorithms, and fuzzy logic control are other MPPT algorithms, which have more complex structures and higher computational loads [7].

A review of the literature reveals numerous studies incorporating MPPT algorithms. In a 2014 study by Vincheh and colleagues, a new hybrid MPPT method was proposed that aims to maximize the efficiency of photovoltaic (PV) systems under rapidly changing environmental conditions. In the study, Neural Network (NN) and Fuzzy Logic Controller (FLC) were used together; the model created was trained with Genetic Algorithm (GA) [8]. In a study conducted by Gülsüm Nazlı Arpacı in 2019, the P&O method, fuzzy logic method, and Adaptive Network-Based Fuzzy Inference method-based MPPT algorithms were compared to determine the best algorithm. The model was designed in the MATLAB/Simulink environment for comparison. She demonstrated that the proposed method has higher efficiency and tracking speed under partial shading conditions [9]. In a study conducted by Irmak and Güler in 2020, a new control strategy was proposed by combining the Perturb & Observe (P&O) algorithm with the Model Predictive Control (MPC) method to improve the dynamic performance of the boost converter used in photovoltaic applications. This developed hybrid method was tested through experimental studies, and its performance was analyzed. According to the results obtained, the proposed approach demonstrated more successful performance in terms of dynamic response; it was noted that it provided a stable and fast transient response, particularly by eliminating the overshoot problem in the system [10]. In a study conducted by Kacimi and colleagues in 2022, they developed a new high-efficiency hybrid algorithm for maximum power point tracking (MPPT) systems operating under variable environmental conditions. The proposed hybrid method consists of a combination of the Grasshopper Optimization Algorithm (GHO) and Model Predictive Control (MPC) techniques. To evaluate the effectiveness of this GHO-MPC-based approach, four different scenarios were created and tested in the MATLAB/Simulink environment [11]. In a study conducted by Gümüş and Demirtaş in 2021, they compared the performance of MPPT under partial shading when run with the P&O, Particle Swarm Optimization (PSO), and Cuckoo Optimization (CSA) algorithms. The comparison revealed that the PSO and CSA algorithms were more successful in reaching the MPP, while the P&O algorithm failed at the maximum point [12]. In a study conducted by Gil-Velasco and Castillo in 2021, they proposed a new MPPT algorithm by adding the ability to search for the global maximum power point in order to improve the Perturb and Observe (P&O) algorithm. This approach aims to reach the maximum power point more efficiently by reducing computational complexity. The developed algorithm was used in conjunction with a boost-type DC-DC converter to step up the voltage obtained from the PV panel to transfer it to the load at specific levels. As a result of the experimental and simulation studies conducted, it was observed that the proposed algorithm successfully tracked the maximum power point within 1.12 seconds [13]. In a study conducted by Baraean and colleagues in 2023, a hybrid maximum power point tracking (MPTT) method was proposed for PV systems operating under variable load and irradiation conditions. This method consists of a combination of an Artificial Neural Network (NN) and an Adaptive Terminal Sliding Mode Control (ATSMC) structure. The method was tested in two different scenarios [14]. In a study conducted by Rania G. Mohamed and colleagues in 2024, a maximum power point tracking (MPPT) method was developed to increase the energy production efficiency of PV panels under partial shading conditions. In this study, Artificial Intelligence (AI) approaches were combined with Fractional Open-Circuit Voltage-based algorithms to enable MPPT to reach the maximum power point more quickly and stably under variable shading conditions [15].

In a study conducted by Benabdallah and colleagues in 2024, a new method was developed that combines adaptive P&O with a hybrid model predictive control (MPC) structure to reduce overshoot and ripple problems that arise during the MPPT process in PV systems. The proposed system suppresses overshoot occurring in transient regimes by responding more quickly to environmental changes and increases stability. Comparative simulation analyses showed lower overshoot, faster stabilisation, and higher efficiency compared to classical P&O and MPC alone [16]. In a study conducted by Prakash and Sahoo in 2015, an interleaved boost converter with soft-switching features was designed to reduce problems such as overshoot, switching losses, and low efficiency observed in classical boost converters in photovoltaic applications. The proposed structure operates with a parallel-connected multi-phase converter topology and zero-current switching (ZCS) technique, thereby reducing overshoot during transient regimes, stabilising the output voltage, and increasing converter efficiency. Simulation and experimental results demonstrate more stable transitions, reduced voltage overshoot, and higher efficiency compared to the classical boost configuration. Converter circuits must be used for the system to operate at its maximum power point. The inductor current in the converter circuits filters the capacitor voltage. Furthermore, controllable switching elements are used to obtain the required current and voltage in the system. In the event of sudden radiation and temperature changes in the system, the system may exhibit an unstable structure for a short period, causing power fluctuations. To stabilise the created system and improve power transfer, literature studies on advanced or multi-level converters have also been encountered [17-19]. In a study conducted by Rongchao Niu and colleagues in 2023, a new Model Predictive Control (MPC) strategy developed specifically to solve the overshoot problem was presented. The high overshoot observed in boost-type converters threatens the stability of the system and the safety of the connected loads. To counter this problem, the method proposed in the paper integrates the Generalised Proportional Integral Observer (GPIO) structure, which can predict time-varying disturbances in real time, with classical MPC [20]. In a study conducted by Paduani et al. in 2023, a maximum power reference tracking (MPRT) algorithm was developed to reduce the output power overshoot problem caused by sudden irradiance changes. The adaptive step size and accumulator mechanism integrated into the classical P&O method suppressed overshoot by regulating the control response when the power reference was exceeded. The simulations performed demonstrated that the proposed method provided lower overshoot, shorter regulation time, and more stable power tracking compared to classical and other adaptive algorithms [21]. In a study conducted by Hang Li and colleagues in 2021, a new design method based on state-space-based overshoot analysis was proposed to systematically predict and limit overshoot in DC–DC converters. The method directly predicts the amount of overshoot that will occur in the output voltage by calculating the maximum deviation in the system's state variables [22].

In this study, an innovative switched boost converter architecture was developed to prevent undesirable effects, particularly transient overshoot and sudden power collapse, arising from transient regime problems in photovoltaic (PV) systems due to variable environmental conditions (e.g., sudden changes in irradiance and temperature values). In traditional boost converters, when operating with a single inductor, capacitor, and load component, sudden changes at the input can directly affect the entire system, resulting in significant fluctuations in output voltage and power. This situation negatively affects the stability of maximum power point tracking (MPPT) algorithms and reduces system efficiency. In the developed structure, switching elements that are activated and deactivated within the scope of a time-dependent control strategy are used. Thanks to these switches, the inductor, capacitor, and load groups are made active or passive according to the system's needs. Thus, in the event of sudden irradiance changes, the circuit topology is dynamically reconfigured, and the energy storage capacity and load equivalent resistance can be optimally adjusted. This approach ensures that the system creates a buffering effect against sudden changes with multiple LC groups connected in parallel and different load configurations. Consequently, thanks to the switched boost converter architecture, instantaneous power drops, overshoot problems, and transient regime fluctuations encountered in single-component classical structures have been significantly reduced, resulting in a more stable and responsive PV power conversion system. This has significantly increased both the efficiency of the system and the tracking accuracy of the MPPT algorithm, particularly under variable environmental conditions.

This study consists of four sections: Introduction, Materials and Methods, Results and Discussion, and Conclusion. The Introduction section details transient regime problems in photovoltaic systems caused by variable environmental conditions and their effects on system performance. A review of the existing literature on the subject is presented, and the purpose, significance, and innovative aspects of the study are highlighted. The Materials and Methods section introduces the photovoltaic panel characteristics used in the study, the boost converter design parameters, the switching strategies employed, and the MPPT algorithms in detail. The methodological approach followed in the study, the circuit topology, the modelling techniques used, and the simulation environment (MATLAB/Simulink) are explained. Furthermore, information is provided on the environmental change scenarios and test conditions. The Findings and Discussion section presents the performance results of the developed switched boost converter structure under different environmental conditions. The obtained data are evaluated with graphs and tables, and comparative analyses with the classical structure are performed. Furthermore, the improvements achieved in terms of reducing transient overshoot, preventing power fluctuations, and increasing system efficiency are discussed in detail. The conclusion section summarises the key findings of the study and highlights the advantages offered by the developed method. Furthermore, recommendations for future work are provided, and assessments are made regarding the adaptability of the developed architecture to different PV system applications.

II. Materials and Method

This section provides a detailed explanation of PV solar panels, solar tracking systems, DC-DC boost converter structure, and MPPT methods, and presents the models created in the study in detail.

A. PV Panel Structure

Solar panels consist of semiconductor materials that can generate electricity using solar radiation [18]. When sunlight hits PV cells, electrons within the semiconductor material are released, generating electrical energy [23]. Figure 1 shows the single diode equivalent circuit of a solar panel [18].

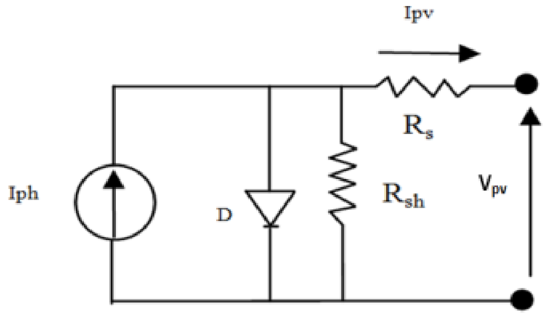

Figure 1. Single diode equivalent circuit of an PV panel

The most fundamental mathematical equation for an ideal PV panel is shown in Equation 1.

$$I_{pv} = I_{ph} - I_0\left[exp\left(\frac{qV_{pv}}{akT}\right) - 1\right] \quad (1)$$

Here, I_{ph} represents the current generated by the sun, I_0 represents the leakage current of the diode, q represents the electron charge, k represents the Boltzmann constant, T represents the temperature, and a represents the diode ideality factor. PV panels are structures formed by combining multiple cells. The equations in Equation 1 have been rearranged, and the mathematical model of the panel is shown in Equation 2 [18].

$$I_{pv} = I_{ph} - I_0\left[exp\left(\frac{V_{pv} + R_sI_{pv}}{V_t a}\right) - 1\right] - \frac{V_{pv} + R_sI_{pv}}{R_{sh}} \quad (2)$$

The equivalent series resistance R_s in Equation 2, the equivalent parallel resistance R_{sh}, and the thermal voltage V_t of the panel are shown in Equation 3. Furthermore, the value I_{pv} in Equation 2 represents point I in the panel's I-V characteristic.

$$V_t = \frac{N_s kT}{q} \quad (3)$$

Equation 3 indicates the number of cells connected in series, N_s. The change in current produced depending on the radiation intensity is shown in Equation 4.

$$I_{ph} = \left(I_{ph,n} + K_I\Delta_T\right)\frac{G}{G_n} \quad (4)$$

The current produced by the PV panel is denoted by I_{ph} and exhibits a linear variation depending on the irradiance value. $I_{ph,n}$ is the current value produced under nominal conditions, i.e., at 25°C and an irradiance value of 1000 W/m². Δ_T represents the difference between the measured and nominal temperature values, while G and G_n represent the measured and nominal radiation values, respectively. The relationship between the diode saturation current and temperature is given in Equation 5 [24].

$$I_0 = I_{0,n}\left(\frac{T_n}{T}\right)^3 exp\left[\frac{qE_g}{ak}\left(\frac{1}{T_n}-\frac{1}{T}\right)\right] \quad (5)$$

The E_g value in Equation 5 represents the semiconductor band energy. $I_{0,n}$ is the nominal saturation current and is expressed in Equation 6.

$$I_{0,n} = \frac{I_{sc,n}}{\exp\left(\frac{V_{oc,n}}{aV_{t,n}}\right)-1} \quad (6)$$

Equation 6 shows that $V_{t,n}$ represents the thermal voltage of the PV panel at nominal temperature.

The current-voltage (I-V) and power-voltage (P-V) characteristics of photovoltaic panels vary directly with environmental conditions such as irradiance and temperature. When examining the I-V curves obtained at different irradiance levels, it is observed that the short-circuit current (I_{sc}) increases significantly with increasing irradiance, while the open-circuit voltage (V_{oc}) increases only to a limited extent. This situation also causes the maximum power point (MPP) in the P-V curves to increase in parallel with irradiance, while only minor changes are observed in the MPP voltage. On the other hand, the I-V and P-V curves obtained at different temperatures reveal that the increase in temperature has a negative effect on V_{oc} and reduces the voltage. As the temperature rises, the panel's MPP voltage decreases, causing the maximum power value to drop, but only minor changes occur in I_{sc}. These findings show that high irradiation levels increase panel power, but high temperatures negatively affect efficiency, and higher power production is possible at lower temperatures.

B. Solar Tracking System

Solar tracking systems are mechanisms developed to ensure that PV panels receive sunlight at the most suitable angle throughout the day. The first solar tracking system was developed by C. Finster in 1927. Although it attempted to detect the sun's position in real time, it had very limited capabilities. Later, in 1963, A. Saavendra designed a system that could automatically detect the sun's position. By 1975, Raymond H. Mcfee had succeeded in determining the sun's position with an accuracy of between 0.5° and 1° using mirrors. The first commercial solar tracking system was developed in 1980 by Mark E. Dorian and David H. Nelson; this system aimed to concentrate the sun's rays at a specific point using collectors. A significant development in tracking systems occurred in 1981 with the use of a microprocessor-based control mechanism by Semma and Imamura. The first computer-aided solar position determination algorithms were developed by Maldonado in 1983 [25]. In light of these developments, various solar tracking strategies have been developed and implemented to obtain maximum efficiency from solar energy.

They are open and closed loop systems according to their control structure. Closed-loop systems operate by applying feedback. This allows the output data to be transferred to the input, enabling control of the panel's position. In open-loop systems, date and time information is provided to the system input, and sun tracking is achieved with the help of algorithms. Active solar tracking systems use electronic systems such as motors and sensors to ensure that the sun is perpendicular to the panel throughout the day. Passive systems do not use electronic components. Instead, tracking is achieved by utilising the expansion of chemical substances [26]. Classification by axis type includes single-axis and dual-axis tracking systems. Figure 2 shows single-axis and dual-axis tracking systems [26].

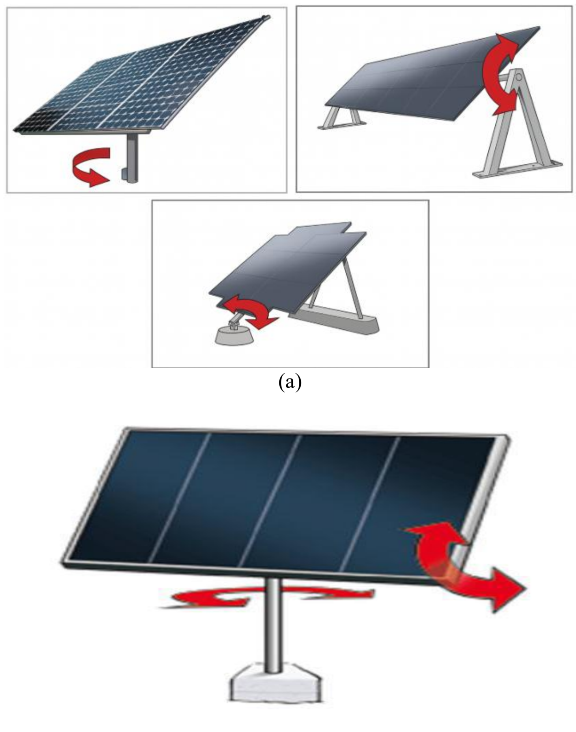

Figure 2. Solar tracking system a) Single-axis solar tracking system b) Dual-axis solar tracking system

In a single-axis tracking system, tracking occurs only on a single axis. That is, tracking is provided only horizontally or vertically. Dual-axis solar tracking systems are capable of both horizontal and vertical movement. Dual-axis tracking systems have a more complex structure than single-axis tracking systems and are also more expensive. However, they are highly successful in terms of high efficiency.

C. DC-DC Boost Converter

These are electronic circuit elements that convert the input voltage to a higher voltage value by utilising the energy stored in the inductor. This is achieved by operating the circuit's control structure to switch the semiconductor element to either the closed or open position [27]. The boost converter structure is shown in Figure 3 [28].

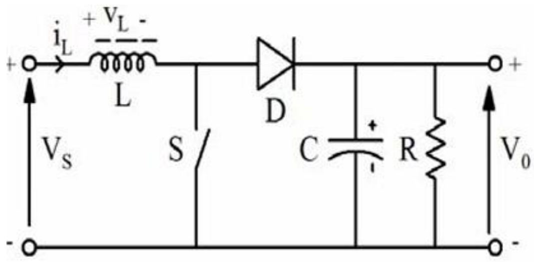

Figure 3. DC-DC boost converter structure

When the switch is in the on state, energy is stored in the coil thanks to the current flowing through the inductor. The switch in the on state is shown in Figure 4a [28].

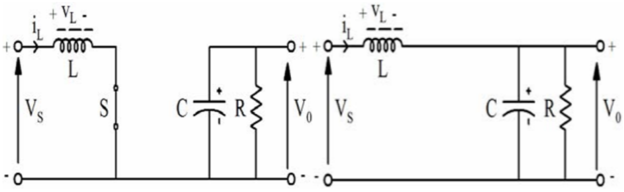

Figure 4. a) Switch in transmission state b) Switch in cut-off state

As soon as the switch turns off, the energy stored in the inductor begins to flow through the diode towards the capacitor and load. The state of the switch being off is shown in Figure 4b. When designing the converter, the values of C_i, L and C_{out} must be calculated. Equation 7 shows the calculation of the inductance value [29].

$$L_{min} \geq \frac{V_{mp}.D}{I_{mp}.\beta.f} \tag{7}$$

Here, V_{mp} denotes the maximum power point voltage, D denotes the duty cycle of the switch, I_{mp} denotes the maximum power point current, β denotes the inductor ripple ratio, and f denotes the frequency. Equation 8 shows the calculation of the input capacitor value [29].

$$C_{i\_min} \geq \frac{D}{8L * \gamma * f^2} \tag{8}$$

Here, D denotes the duty cycle, L denotes the inductance value, γ denotes the inductor ripple ratio, and f denotes the frequency. Equation 9 shows the calculation of the output capacitor value [29].

$$C_{out\_min} \geq \frac{D}{R_0 * \gamma * f} \tag{9}$$

Here, D denotes the duty cycle of the switch, R_0 denotes the output resistance, γ denotes the inductor ripple ratio, and f denotes the frequency.

D. Maximum Power Point Tracker

The voltage and current values obtained from photovoltaic panels vary depending on the temperature, radiation, and partial shading conditions on the panel surface [30]. It is desired that photovoltaic panels operate at the maximum power point under all conditions. Thanks to maximum power point algorithms, the voltage and current produced by the panel are continuously monitored, aiming to ensure that the system always operates at the maximum power point. Many methods and algorithms have been developed to find the maximum power point of a photovoltaic system. The developed methods are generally classified as intelligent, traditional, hybrid, and metaheuristic [31]. Although traditional methods are preferred due to their low cost and simplicity, they may not perform well in determining the maximum power point during sudden irradiance changes and partial shading conditions [32].

Among the classical algorithms, the Perturb-Observe algorithm is one of the preferred algorithms due to its simple structure, applicability, and few parameters [33-34]. This algorithm operates the system at the ideal point based on voltage and power values. In the Perturb-Observe algorithm, the current and voltage values of the panel are first measured. The power of the panel is calculated from the measured values. If ΔP=0, the cycle returns to the beginning. When $\Delta P < 0$, it is checked whether the V_k value is greater or less than the V_{k-1} value. If $V_k > V_{k-1}$, the V_{ref} value is decreased. If $V_k < V_{k-1}$, the V_{ref} value is increased. When $\Delta P > 0$, if $V_k > V_{k-1}$, the V_{ref} value is increased. If $V_k < V_{k-1}$, the V_{ref} value is decreased.

The Incremental Conductance algorithm is a frequently preferred method in MPPT applications due to its ability to quickly adapt to changing environmental conditions [35]. The IC algorithm is based on the condition that the derivative of the PV panel's output power with respect to voltage is zero. In the PV system, the derivative of power with respect to voltage is equal to zero at MPP. Equation 10 provides the mathematical equations for the IC algorithm.

$$\frac{dP_{FV}}{dV_{FV}} = \frac{d(I_{FV}V_{FV})}{dV_{FV}} = I_{FV} + V_{FV}\frac{dI_{FV}}{dV_{FV}} \tag{10}$$

The case where the derivative is zero in MPP is shown in Equation 11.

$$\frac{dI_{FV}}{dV_{FV}} = -\frac{I_{FV}}{V_{FV}} \tag{11}$$

When MPP remains on the left, the current-to-voltage ratio is negative, whereas it is positive when it remains on the right. The IC algorithm ensures the system operates in MPP by comparing the instantaneous conductivity value $\left(\frac{I}{V}\right)$ with the incremental conductance value $\left(\frac{\Delta I}{\Delta V}\right)$ [31].

The Particle Swarm Optimisation (PSO) algorithm is an heuristic optimisation method with few parameters and fast convergence capability, where candidate solutions, each acting as a particle in the solution space, continuously update their velocity and position to converge towards the global optimum solution. Therefore, PSO provides higher tracking speed and stable power production compared to classical methods in maximum power point tracking applications in photovoltaic (PV) systems [36]. The position and velocity of each particle in the PSO algorithm are shown in Equation 12.

$$\mathrm{v}_i^{k+1} = \omega\, \mathrm{v}_i^k + c_1 r_1^k\left(\mathrm{p}_i^k - \mathrm{x}_i^k\right) + c_2 r_2^k\left(\mathrm{g}^k - \mathrm{x}_i^k\right)$$
$$\mathrm{x}_i^{k+1} = \mathrm{x}_i^k + \mathrm{v}_i^{k+1} \tag{12}$$

Here; x_i is the particle's position, v_i is the particle's velocity, p_i is the particle's best position so far (pbest), g is the best position in the swarm (gbest), ω is the inertia coefficient, c_1 and c_2 are cognitive and social coefficients, r_1^k and r_2^k are random values in the range [0,1].

The updating of the best values when the power evaluation function is minimised is shown in Equation 13.

$$\mathrm{p}_i^{k+1} = \begin{cases} \mathrm{x}_i^{k+1}, & J(\mathrm{x}_i^{k+1}) < J(\mathrm{p}_i^k) \\ \mathrm{p}_i^k, & \text{diğer durumlar} \end{cases} \qquad \mathrm{g}^{k+1} = \arg\min_j J\left(\mathrm{p}_j^{k+1}\right) \tag{13}$$

In the PSO algorithm used for maximum power point tracking in photovoltaic systems, the power evaluation function is defined to maximise the panel output power. The maximisation problem is converted into a minimisation form as shown in Equation 14.

$$J(\mathrm{x}) = -P_{\mathrm{PV}}(\mathrm{x}) = -V_{\mathrm{PV}}(\mathrm{x})\, I_{\mathrm{PV}}(\mathrm{x}) \tag{14}$$

Here, x typically represents the PV panel voltage (V_{ref}) or the converter duty ratio (D). In applications based on boost converters, the optimal duty ratio D_{opt} is obtained as a result of the above updates.

In the hybrid structure where PSO and increasing conductance algorithms are used together, the PSO algorithm searches for the global maximum power point, while the Incremental Conductance (IC) method provides local accuracy and stability. In the PSO phase, particles roam at different duty cycles to find the highest power value; this point is transferred to the IC phase. In the IC phase, the system is fine-tuned to the maximum power point by satisfying the condition $\frac{dI}{dV} = -\frac{I}{V}$. The hybrid structure combines the wide search capability of PSO with the low oscillation advantage of IC. This results in shorter settling time, low ripple, and high tracking efficiency. Studies show that the PSO+IC method provides faster and more stable results compared to classical P&O and standalone IC [37-39].

E. Performance Metrics

The most common statistical performance indicators used to evaluate the accuracy and stability of MPPT algorithms in PV systems are RMSE (Root Mean Squared Error), MAPE (Mean Absolute Percentage Error) and ripple percentage (Ripple%). These error metrics provide an objective means of comparing the effectiveness of algorithms by numerically defining the difference between the power values predicted (or tracked) by the system and the actual power.

Root Mean Squared Error (RMSE) is the square root of MSE with the unit preserved. Its mathematical expression is shown in Equation 15.

$$RMSE = \sqrt{\frac{1}{N}\sum_{i=1}^{N}(y_i - \hat{y}_i)^2} \tag{15}$$

The RMSE value expresses the average deviation of the estimated power values from the actual values in the system's own units (e.g., Watt). In this respect, it enables the physical evaluation of MPPT performance. The lower the RMSE value, the faster, more stable, and more accurate the algorithm is in tracking. In the literature, PSO, Fuzzy, and IC-based MPPT studies have considered RMSE as an important indicator of system stability and convergence success [38-39].

The Mean Absolute Percentage Error (MAPE) is a relative error measure that expresses the difference between the predicted and actual values as a percentage. Its mathematical expression is shown in Equation 16.

$$MAPE = \frac{100\%}{N}\sum_{i=1}^{N} \left| \frac{y_i - \hat{y}_i}{y_i} \right| \tag{16}$$

MAPE is used to compare the tracking efficiency of MPPT algorithms operating under different irradiation conditions. Its percentage expression format facilitates performance evaluations between different systems or panels. A low MAPE value indicates that the system exhibits high accuracy and a low relative error rate in power estimation. The literature emphasises that MAPE is an important metric for evaluating the sensitivity of PV systems to dynamic changes [34], [40].

Ripple Percentage (Ripple%) is a stability indicator that shows the ratio of fluctuations in the converter output power, voltage, or current to the average value. Mathematically, as shown in Equation 17, the ripple percentage is the percentage expression of the peak-to-peak variation normalised to the average power.

$$\text{Ripple}(\%) = \frac{P_{\max} - P_{\min}}{P_{\text{avg}}} \times 100 \tag{17}$$

Here, $P_{\max}$ and $P_{\min}$ represent the maximum and minimum values of the converter output power within a time window, while P_{avg} indicates the average power. A low ripple percentage indicates that the output is smoother (more stable) and that the system behaves more stably against sudden transitions or radiation changes. Therefore, Ripple% is frequently used in evaluating not only the tracking accuracy of MPPT algorithms but also the dynamic stability of converter-based PV systems [38], [41-42].

III. RESULTS

In this study, the classical boost converter was compared with a switched adaptive converter structure, whose C_{in}, C_{out}, and L values vary over time, under different irradiance and temperature values that change throughout the day. In the study, the obtained irradiance data were first used to obtain effective radiation values using a dual-axis solar tracking system designed in the MATLAB/Simulink environment. The structure designed in the MATLAB/Simulink environment is shown in Figure 5.

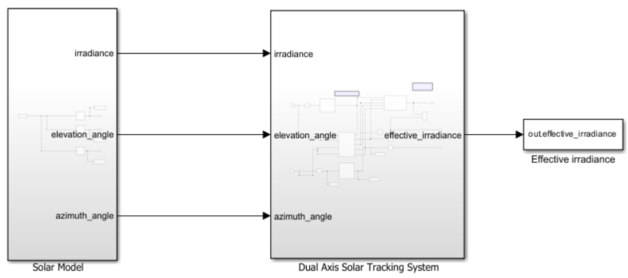

Figure 5. Dual-axis solar tracking system designed in the MATLAB/Simulink environment

The effective radiation values obtained were applied to the input of the KC200GT photovoltaic panel designed using a mathematical model in the MATLAB/Simulink environment. The photovoltaic panel design obtained using the mathematical model is shown in Figure 6.

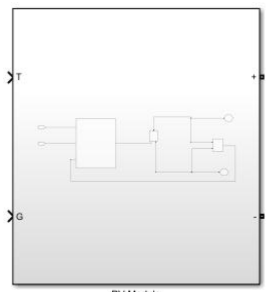

(a)

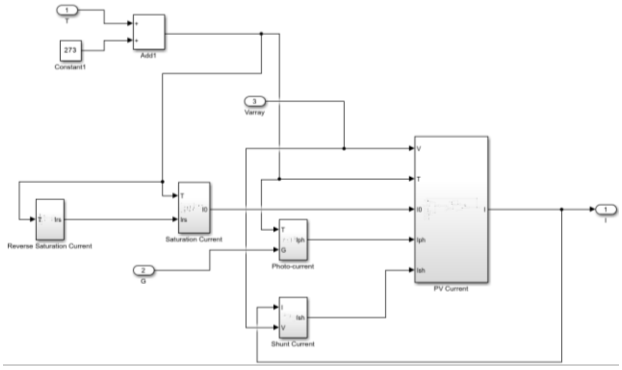

(b)

Figure 6. Structure designed using a mathematical model in the MATLAB/Simulink environment a) General view b) Internal structure

The system parameters under the nominal temperature and radiation values of the PV panel are given in Table 1.

Table 1. KC200GT PV panel parameter values

Parameter	Value
I_{mp}	7.61 A
V_{mp}	26.3V
$P_{max,m}$	200.143 W
I_{sc}	8.21 A
V_{oc}	32.9 V
$I_{o,n}$	8.214 A
a	1.3
K_v	-0.1230V/K
K_I	0.0032A/K
N_s	54
R_p	415.405 Ω
R_s	0.221 Ω

The I-V and P-V characteristics of the system designed in MATLAB/Simulink were generated at different temperature and irradiance values. The I-V and P-V characteristics of the model generated at 25°C under irradiance values of 1000 W/m², 750 W/m², and 500 W/m² are shown in Figure 7.

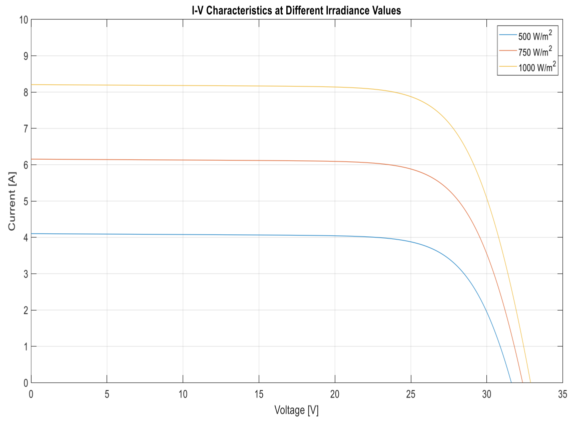

(a)

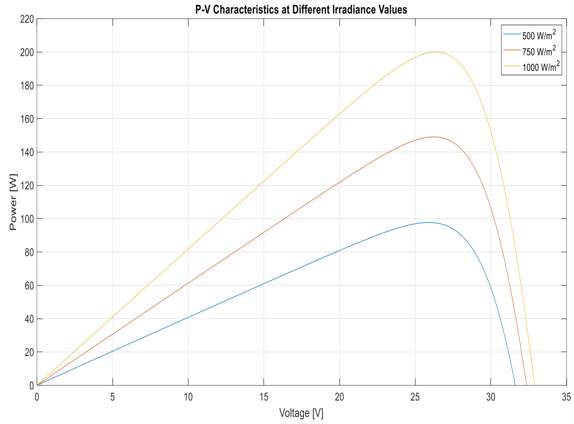

(b)

Figure 7. (a) I-V and (b) P-V characteristics at a constant temperature under different irradiance values

The graphs obtained in the study conducted at different temperatures under a constant radiation value are shown in Figure 8. The graphs obtained at temperatures of 15°C, 25°C, and 45°C at a radiation value of 1000 W/m² are shown.

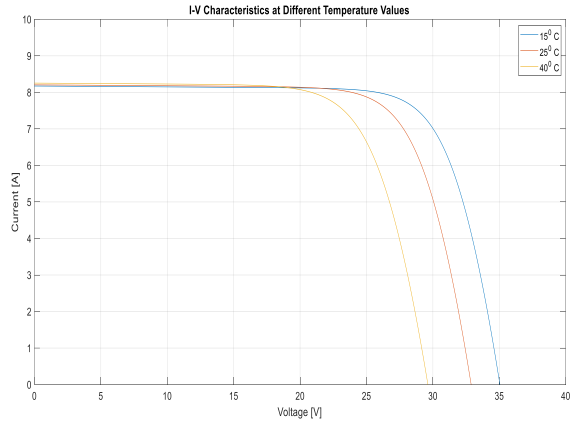

(a)

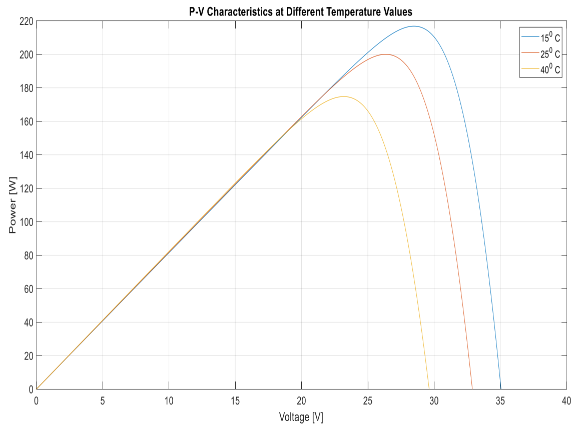

(b)

Figure 8. (a) I-V and (b) P-V characteristics at different temperatures under constant irradiance values

The voltage level of the designed PV system is increased with the help of a boost converter, ensuring that the system operates at its maximum power point. The classic boost converter structure designed in the MATLAB/Simulink environment is shown in Figure 9.

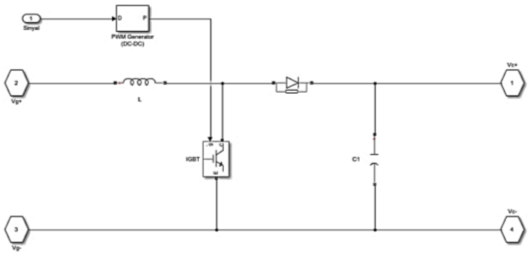

Figure 9. Classic boost converter structure designed in the MATLAB/Simulink environment

To verify the accuracy of the designed boost converter structure, the output values were observed using data obtained from the load via a fixed DC voltage source and signal generator. This is shown in Figure 10.

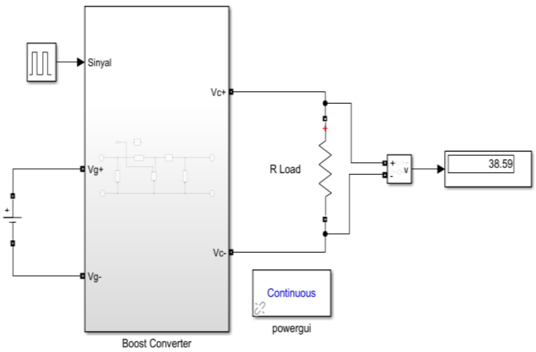

(a)

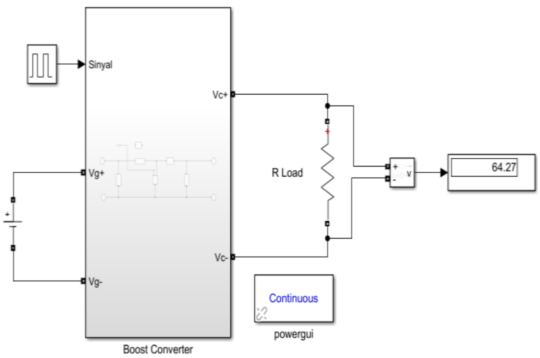

(b)

Figure 10. Boost converter structure created using a fixed DC voltage source a) D= 0.5 b) D=0.7

In the structure shown in Figure 10a, the input voltage was set to 20 V and the signal generator was set to 50%, i.e. the duty cycle D = 0.5. The system output was approximately 40 V. Losses in the system prevented us from reaching exactly 40 V. In the structure shown in Figure 10b, the input voltage was set to 20 V, and the signal generator was set to 70%, i.e., the duty cycle D = 0.7. The system output was approximately 66 V. The losses occurring in the system prevented us from reaching exactly 66 V. These results prove the accuracy of the designed boost converter structure.

The adaptive converter structure shown in Figure 11 significantly improves the problems of spiking, overshoot, and ripple that occur in classic boost converters at different radiation and temperature values.

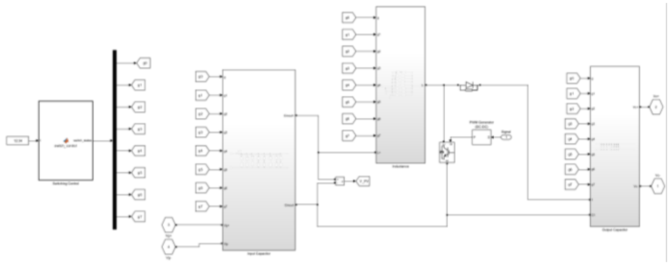

Figure 11. Designed adaptive boost converter structure

In the structure shown in Figure 11, specific capacitors and inductors are connected to the circuit according to each time interval. Which capacitor and inductor will be active in which time interval is determined by the switch controller seen on the left side of Figure 11. It activates or deactivates the switches according to the order we defined earlier. In the switch control structure shown in Table 2, the activation or deactivation status of each LC group is determined by a time-based switching logic. For this purpose, each switch status has been defined. Here, a value of 1 indicates that the relevant LC group is active, while a value of 0 indicates that it is inactive. In this study, the total number of LC groups is denoted by N, and N=8 has been adopted for the proposed structure.

Table 2. Changes in the positions of the main characters over time

Changes in Keys Over Tıme	
Time	**Switching States**
0-1	[1 0 0 0 0 0 0 0]
1-2	[1 1 0 0 0 0 0 0]
2-3	[1 1 1 0 0 0 0 0]
3-4	[1 1 1 1 0 0 0 0]
4-5	[1 1 1 1 1 0 0 0]
5-6	[1 1 1 1 1 1 0 0]
6-7	[1 1 1 1 1 1 1 0]
7-8	[1 1 1 1 1 1 1 0]
8-9	[1 1 1 1 1 1 1 0]
9-10	[1 1 1 1 1 1 0 0]
10-11	[1 1 1 1 1 0 0 0]
11-12	[1 1 1 1 0 0 0 0]
12-13	[1 1 1 0 0 0 0 0]
13-14	[1 1 0 0 0 0 0 0]
14-15	[1 0 0 0 0 0 0 1]

In the June operating scenario, the total analysis time was set at 15 hours. Within each one-hour time interval, the switch states were changed according to a predefined sequence. Consequently, the active LC groups in the adaptive boost converter configuration vary over time, and the system's equivalent inductance and capacitance values are recalculated for each time interval. Due to the time-dependent variation of the switching states, the equivalent circuit parameters in the proposed converter structure are not constant. Consequently, unlike a conventional boost converter, the system exhibits a time-varying, switched structure. The equivalent inductance and equivalent capacitance values resulting from the active switching positions are defined in Equation 18.

$$\begin{cases} i = 1,2,\dots,N \\ L_{eq}(t) = \left(\sum_{i=1}^{N} \frac{S_i(t)}{L_i}\right)^{-1} \\ C_{eq} = \sum_{i=1}^{N} S_i(t) C_i \end{cases} \quad (18)$$

In this equation, N denotes the total number of LC groups, $S_i(t)$ denotes the state of the i-th switch, and L_i, C_i denote the element values belonging to the i-th group. In time intervals where radiation and temperature values are close to one another, the positions of the switches have not been altered. This structure forms a time-varying, switch-based system. The state equations of the designed system are given in Equation 19.

$$x_1 = i_{L,} \quad x_2 = V_0 \tag{19}$$

In this case, the system's state variables have been selected as the inductor current and the output voltage, and the state vector is defined as in Equation 20.

$$x(t) = \begin{bmatrix} i_L(t) \\ V_0(t) \end{bmatrix} \tag{20}$$

The state equations for the designed system are given in Equation 21.

$$\begin{cases} \dfrac{di_L}{dt} = \dfrac{V_{pv} - (1-D).V_0}{L_{eq}(t)} \\ \dfrac{dV_0}{dt} = \dfrac{(1-D).i_L - \dfrac{V_0}{R_L}}{C_{eq}(t)} \end{cases} \tag{21}$$

These resulting state equations demonstrate that the proposed adaptive boost converter is a non-linear system whose parameters vary depending on the switching state. Since the inductance and capacitance values, which are fixed in the classical boost converter, vary according to the active switch combination in the proposed configuration, the system exhibits different dynamic behaviour across its operating range. An overview of the designed system is shown in Figure 12.

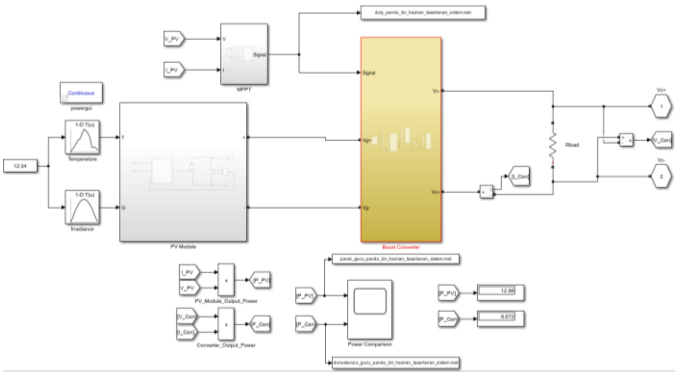

Figure 12. General view of the system designed in MATLAB/Simulink

As a result of this designed system, a comparison of the power data output for the conventional converter and the converter we designed was performed using three different MPPT methods. The MPPT methods used are PandO, IC, and PSO+IC.

The values obtained from the analysis using a single-value conventional converter and adaptive converter structure consisting of one C_{in}, L, and C_{out} value as a result of the PandO algorithm are shown in Table 3.

Table 3. Panel and converter power values of the conventional converter and the designed adaptive converter as a result of the PandO algorithm

Comparison of PandO Algorithms According to Converter Type					
Time	**Irradiance (W/m²)**	**Temperature (°C)**	**Converter Type**	**Average Panel Power (W)**	**Average Converter Power (W)**
1	89.64	14.1	**Classic Converter**	16.263	15.495
			Designed Converter	16.297	15.695
2	308.99	15.3	**Classic Converter**	63.396	60.498
			Designed Converter	63.508	60.793
3	549.61	16.2	**Classic Converter**	115.820	111.321
			Designed Converter	115.950	111.549
4	775	17.6	**Classic Converter**	163.613	157.632
			Designed Converter	163.689	158.056
5	969.47	18.9	**Classic Converter**	203.503	196.500
			Designed Converter	203.546	197.045
6	1119.9	19.2	**Classic Converter**	234.794	227.116
			Designed Converter	234.777	227.650
7	1216.3	21.1	**Classic Converter**	251.175	243.584
			Designed Converter	251.091	243.743
8	1251.5	23	**Classic Converter**	254.429	246.974
			Designed Converter	254.359	247.044
9	1223.3	22.4	**Classic Converter**	249.947	241.908
			Designed Converter	249.887	242.648
10	1134.3	21.5	**Classic Converter**	233.470	225.777
			Designed Converter	233.452	226.536
11	990.2	20	**Classic Converter**	206.055	199.094
			Designed Converter	206.084	199.734
12	800.68	16	**Classic Converter**	171.295	165.138
			Designed Converter	171.400	165.726
13	578.53	16	**Classic Converter**	122.397	117.604
			Designed Converter	122.519	118.062
14	339.29	16	**Classic Converter**	69.651	66.563
			Designed Converter	69.795	66.919
15	129.32	15	**Classic Converter**	24.479	23.251
			Designed Converter	24.530	23.466

The single-valued converter resulting from the PandO algorithm and the power graph of the designed converter and panel are shown in Figure 13.

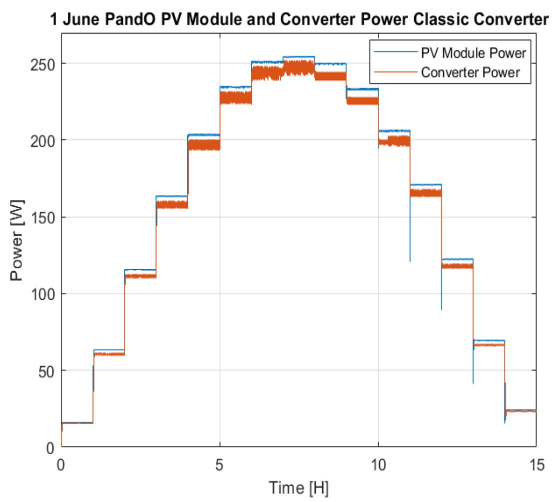

(a)

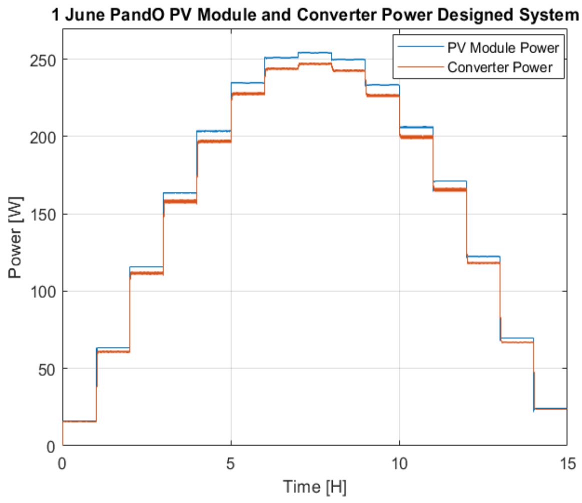

(b)

Figure 13. For the PandO algorithm: a) Comparison of panel and converter power in the classical converter b) Comparison of panel and converter power in the designed adaptive converter

Figure 13a shows the power graph obtained using the classic converter structure. Downward spikes in panel power are present at certain points on the graph. Furthermore, when examining the converter power in this system, significant fluctuations in converter power are observed, particularly at high power levels. The adaptive converter structure we designed under the same temperature and irradiance values is shown in Figure 13b. The fluctuations in panel power have disappeared, and it can be seen that the oscillations in converter power, especially at high power levels, have decreased. The results obtained when examining some signal characteristics and the efficiency of these two systems are given in Table 4.

Table 4. Comparison of signal characteristics and efficiency between the classical and adaptive systems for the PandO algorithm

Values Produced by the PandO Algorithm				
	RMSE	MAPE	Converter Ripple (%)	Efficiency
Classic Converter	5.596	3.756	3.179	96.243
Designed Converter	5.110	3.438	1.181	96.560

When examining the signal characteristics of the classical and designed converters, the root mean square error value for the classical system is 5.596, while the value for the adaptive system is calculated as 5.110. When examining the systems in terms of average absolute percentage error, the value for the classical system is 3.756, while the value for the adaptive system is calculated as 3.438. When the converter output power fluctuation is examined in percentage terms, the fluctuation in the classical system is 3.179%, while the value in the adaptive system is calculated as 1.181%. When the two systems are examined in terms of efficiency, the efficiency of the classical system is 96.243, while the efficiency value of the adaptive system is 96.560. These calculated values were obtained by taking the average values for the entire duration of the panel's exposure to sunlight.

The values obtained from the single-value classical converter and adaptive converter analysis performed using the IC algorithm are shown in Table 5.

Table 5. Panel and converter power values of the conventional converter and the designed adaptive converter as a result of the IC algorithm

Comparison of IC Algorithms According to Converter Type					
Time	Irradiance (W/m²)	Temperature (°C)	Converter Type	Average Panel Power (W)	Average Converter Power (W)
1	89.64	14.1	Classic Converter	16.264	15.498
			Designed Converter	16.297	15.695
2	308.99	15.3	Classic Converter	63.394	60.485
			Designed Converter	63.507	60.795
3	549.61	16.2	Classic Converter	115.823	111.278
			Designed Converter	115.958	111.550
4	775	17.6	Classic Converter	163.618	157.773
			Designed Converter	163.702	158.074
5	969.47	18.9	Classic Converter	203.506	196.663
			Designed Converter	203.546	197.042
6	1119.9	19.2	Classic Converter	234.800	227.201
			Designed Converter	234.799	227.650
7	1216.3	21.1	Classic Converter	251.117	243.225
			Designed Converter	251.137	243.794
8	1251.5	23	Classic Converter	254.424	246.760
			Designed Converter	254.367	247.048
9	1223.3	22.4	Classic Converter	249.946	241.918
			Designed Converter	249.863	242.643
10	1134.3	21.5	Classic Converter	233.470	225.784
			Designed Converter	233.455	226.543
11	990.2	20	Classic Converter	206.062	199.131
			Designed Converter	206.129	199.773
12	800.68	16	Classic Converter	171.297	165.169
			Designed Converter	171.375	165.697
13	578.53	16	Classic Converter	122.404	117.634
			Designed Converter	122.527	118.069
14	339.29	16	Classic Converter	69.669	66.525
			Designed Converter	69.795	66.920
15	129.32	15	Classic Converter	24.479	23.255
			Designed Converter	24.531	23.468

The power graph obtained from the analysis using the classical converter and adaptive converter structures as a result of the IC algorithm is shown in Figure 14.

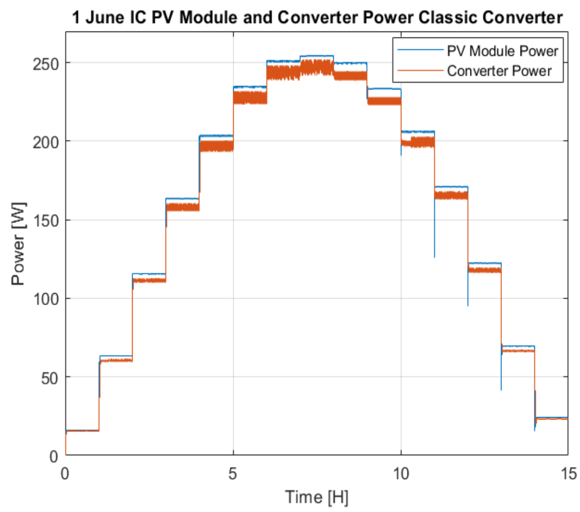

(a)

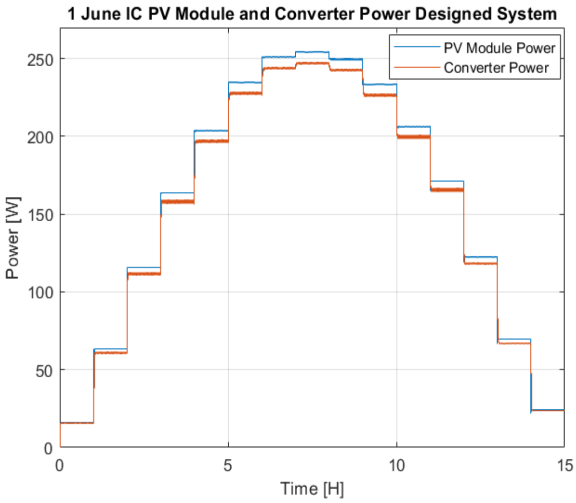

(b)

Figure 14. For the IC algorithm: a) Comparison of panel and converter power in the classical converter b) Comparison of panel and converter power in the designed adaptive converter

Figure 14a shows the power graph obtained using the classical converter structure. At certain points on the graph, downward spikes in panel power are present, as in the PandO algorithm. Furthermore, when examining the converter power in this system, significant fluctuations in converter power are observed, particularly at high power levels, as in the PandO algorithm. The adaptive converter structure we designed under the same temperature and irradiance values is shown in Figure 14b. The dips in panel power have disappeared, and it can be seen that the oscillations in converter power, especially at high power levels, have decreased. The results obtained when examining some signal characteristics and the efficiency of the system for these two systems are given in Table 6.

Table 5. Comparison of signal characteristics and efficiency between the classical and adaptive systems for the IC algorithm

Values Produced by the IC Algorithm				
	RMSE	MAPE	Converter Ripple (%)	Efficiency
Classic Converter	5.611	3.760	3.181	96.239
Designed Converter	5.110	3.439	1.177	96.560

When examining the signal characteristics of the classical and designed converters, the root mean square error value for the classical system is 5.611, while the adaptive system's value is calculated as 5.110. When examining the systems in terms of the mean absolute percentage error, the value for the classical system is 3.760, while the value for the adaptive system is calculated as 3.439. When examining the converter output power fluctuation in percentage terms, the fluctuation in the classical system is 3.181%, while the value in the adaptive system is calculated as 1.177%. When the two systems were examined in terms of efficiency, the efficiency of the classical system was 96.239, while the efficiency value of the adaptive system was 96.560.

The PSO parameters used in the hybrid PSO+IC algorithm were determined as follows: the number of particles was selected as 5, the inertia weight as $w = 0.5$, the cognitive coefficient as $c_1 = 1.3$, and the social coefficient as $c_2 = 1.5$. In addition, the duty cycle search range was limited between 0.05 and 0.95. The values obtained from the single-valued classical converter and adaptive converter analysis performed using the PSO+IC algorithm are shown in Table 7.

Table 7. Panel and converter power values of the conventional converter and the designed adaptive converter as a result of the PSO+IC algorithm

Comparison of PSO+IC Algorithms According to Converter Type					
Time	Irradiance (W/m²)	Temperature (°C)	Converter Type	Average Panel Power (W)	Average Converter Power (W)
1	89.64	14.1	Classic Converter	16.282	15.508
			Designed Converter	16.304	15.702
2	308.99	15.3	Classic Converter	63.448	60.604
			Designed Converter	63.518	60.799
3	549.61	16.2	Classic Converter	115.906	111.243
			Designed Converter	115.995	111.587
4	775	17.6	Classic Converter	163.674	157.882
			Designed Converter	163.752	158.121
5	969.47	18.9	Classic Converter	203.579	196.556
			Designed Converter	203.628	197.121
6	1119.9	19.2	Classic Converter	234.906	227.248
			Designed Converter	234.932	227.794
7	1216.3	21.1	Classic Converter	251.283	243.459
			Designed Converter	251.257	243.910
8	1251.5	23	Classic Converter	254.519	246.773
			Designed Converter	254.532	247.202
9	1223.3	22.4	Classic Converter	250.059	242.311
			Designed Converter	250.039	242.811
10	1134.3	21.5	Classic Converter	233.563	226.151
			Designed Converter	233.583	226.669
11	990.2	20	Classic Converter	206.169	199.216
			Designed Converter	206.202	199.851
12	800.68	16	Classic Converter	171.411	165.268
			Designed Converter	171.456	165.780
13	578.53	16	Classic Converter	122.483	117.658
			Designed Converter	122.563	118.102
14	339.29	16	Classic Converter	69.732	66.564
			Designed Converter	69.805	66.932
15	129.32	15	Classic Converter	24.508	23.28
			Designed Converter	24.537	23.474

The power graph resulting from the analysis using the classical converter and adaptive converter structure based on the PSO + IC hybrid algorithm is shown in Figure 15.

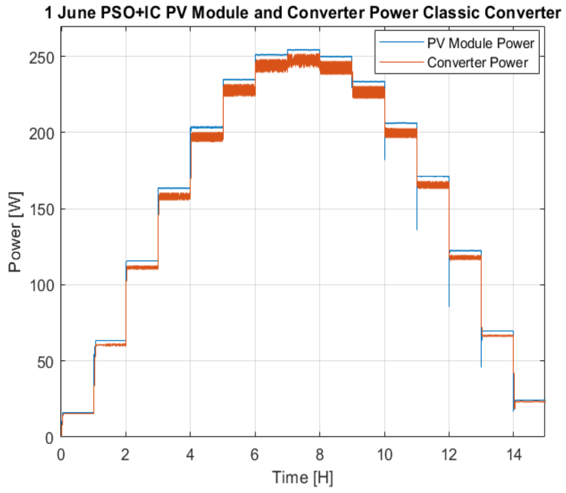

(a)

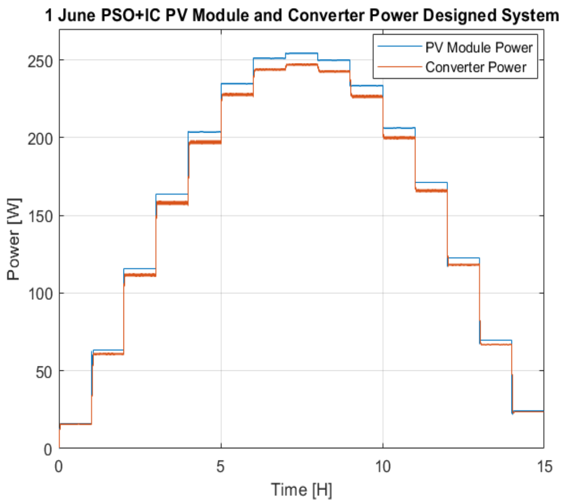

(b)

Figure 15. For the PSO+IC algorithm: a) Comparison of panel and converter power in the classical converter b) Comparison of panel and converter power in the designed adaptive converter

Figure 15a shows the power graph obtained using the classical converter structure. At certain points on the graph, downward spikes in panel power are present, as in the PandO and IC algorithms. Furthermore, when examining the converter power in this system, significant fluctuations in converter power are observed, particularly at high power levels, as in the PandO and IC algorithms. The adaptive converter structure we designed under the same temperature and irradiance values is shown in Figure 15b. The fluctuations in panel power have disappeared, and it can be seen that the oscillations in converter power, especially at high power levels, have decreased. The results obtained when examining some signal characteristics and the efficiency of these two systems are given in Table 8.

Table 8. Comparison of signal characteristics and efficiency between the classical and adaptive systems for the PSO + IC algorithm

Values Produced by the PSO+IC Algorithm				
	RMSE	MAPE	Converter Ripple (%)	Efficiency
Classic Converter	5.642	3.757	3.148	96.242
Designed Converter	5.109	3.438	1.038	96.561

When examining the signal characteristics of the classical and designed converters, the root mean square error value for the classical system is 5.642, while the adaptive system's value is calculated as 5.109. When examining the systems in terms of the mean absolute percentage error, the value for the classical system is 3.757, while the value for the adaptive system is calculated as 3.438. When examining the converter output power fluctuation percentage, the fluctuation in the classical system is 3.148%, while the value in the adaptive system is calculated as 1.038%. When examining the two systems in terms of efficiency, the efficiency of the classical system is 96.242, while the efficiency value of the adaptive system is 96.561.

IV. CONCLUSION

In this study, a time-dependent switched adaptive boost converter architecture has been developed as an alternative to the classical boost converter topology to reduce transient regime problems caused by variable irradiance and temperature conditions in photovoltaic (PV) systems. The designed system operates under a constant load and relies on the time-based switching control of inductor and capacitor groups to adapt to different environmental conditions. This ensures high stability in power transfer.

In simulations performed in the MATLAB/Simulink environment, the proposed converter structure was compared with the classical structure under P&O, IC, and PSO+IC algorithms. The results obtained show that the proposed system operates with lower root mean square error (RMSE), smaller mean absolute percentage error (MAPE), and lower converter power ripple in all three algorithms.

In particular, the adaptive converter structure operated with the PSO+IC hybrid MPPT algorithm provided the highest performance with a tracking efficiency of 96.5612%, unlike the classical structure. By combining the global search capability of PSO and the local accuracy advantage of IC, both the convergence time and the amount of oscillation of the system were reduced. This resulted in a noticeable improvement in power transfer for the system operating under a constant load.

The spiking, overshoot, and oscillation problems observed in the conventional converter structure, particularly at high irradiance values, were significantly suppressed thanks to the developed time-dependent switching structure. Dynamic LC element transitions have prevented transient regime instabilities during sudden irradiance changes and ensured continuity in the system's output power. This has increased the tracking accuracy of the MPPT algorithm and improved the overall energy efficiency of the PV system.

In tests conducted under different irradiation and temperature scenarios, the adaptive structure maintained stable power transfer. The time-dependent change in circuit topology enabled the system to respond more flexibly and quickly to environmental effects. Thus, a larger portion of the power generated by the PV panel was transferred to the load.

Consequently, the developed time-dependent switched adaptive boost converter architecture demonstrated significant superiority in terms of stability, accuracy, and efficiency compared to classical structures. When integrated with MPPT algorithms, it enabled the system to find the maximum power point more accurately and quickly, minimising transient regime effects. Particularly when combined with the PSO+IC hybrid method, the proposed structure operated more stably, with lower error values and higher energy efficiency in both transient and steady-state regimes. Future work should focus on implementing the developed system in real time at the hardware level and comparing it with different meta-heuristic algorithms (e.g., GWO, GA, SSA, etc.).

REFERENCES

[1] T.C. Enerji ve Tabii Kaynaklar Bakanlığı, "Elektrik," Bilgi Merkezi Enerji, [Online]. Available: https://enerji.gov.tr/bilgi-merkezi-enerji-elektrik. Accessed: Oct. 27, 2025.

[2] K. Javed, H. Ashfaq, and R. Singh, "An Improved MPPT Algorithm to Minimize Transient and Steady State Oscillation Conditions for Small SPV Systems," *International Journal of Renewable Energy Development (IJRED)*, vol. 7, no. 3, pp. 191–197, 2018. doi: 10.14710/ijred.7.3.191-197.

[3] B. Liu, S. Duan, F. Liu, and Y. Kang, "A variable step size INC MPPT method for PV systems," *IEEE Trans. Ind. Electron.*, vol. 55, no. 7, pp. 2622–2628, Jul. 2011.

[4] Z. Li, S. Kai, X. Yan, F. Lanlan, and H. Guo, "A modular grid-connected photovoltaic generation system based on DC bus," *IEEE Trans. Power Electron.*, vol. 26, no. 2, pp. 523–531, Feb. 2011.

[5] J. L. Agorreta, M. Borrega, J. López, and L. Marroyo, "Modeling and control of N-paralleled grid-connected inverters with LCL filter coupled due to grid impedance in PV plants," *IEEE Trans. Power Electron.*, vol. 26, no. 3, pp. 770–785, Mar. 2011.

[6] Y. Bo, W. Liu, Y. Zhang, and X. He, "Design and analysis of a grid-connected photovoltaic power system," *IEEE Trans. Power Electron.*, vol. 25, no. 4, pp. 992–1000, Apr. 2010.

[7] A. Saberi, M. Niroomand, and B. M. Dehkordi, "An improved P&O based MPPT for PV systems with reduced steady-state oscillation," *Int. J. Energy Res.*, vol. 47, no. ?, pp. 1–15, Jul. 2023, doi: 10.1155/2023/4694583.

[8] M. R. Vincheh, A. Kargar, and G. A. Markadeh, "A hybrid control method for maximum power point tracking (MPPT) in photovoltaic systems," *Arabian J. Sci. Eng.*, vol. 39, pp. 4715–4725, 2014.

[9] G. N. Arpacı, "Design and comparison of Perturb & Observe, Fuzzy Logic and ANFIS based MPPT controller for PV system," M.S. thesis, Dept. of Electrical and Electronics Eng., Gazi Univ., Ankara, Turkey, 2019.

[10] E. Irmak and N. Güler, "A model predictive control-based hybrid MPPT method for boost converters," *Int. J. Electron.*, vol. 107, no. 1, pp. 1–16, 2020.

[11] N. Kacimi, A. Idir, S. Grouni, and M. S. Boucherit, "A new combined method for tracking the global maximum power point of photovoltaic systems," *Rev. Roum. Sci. Tech. – Série Électrotech. Énerg.*, vol. 67, no. 3, pp. 349–354, 2022.

[12] Z. Gümüş and M. Demirtaş, "Fotovoltaik sistemlerde maksimum güç noktası takibinde kullanılan algoritmaların kısmi gölgeleme koşulları altında karşılaştırılması," *Politeknik Dergisi*, vol. 24, no. 3, pp. 853–865, 2021.

[13] A. Gil-Velasco and C. Aguilar-Castillo, "A modification of the perturb and observe method to improve the energy harvesting of PV systems under partial shading conditions," *Energies*, vol. 14, no. 9, Art. no. 2521, 2021.

[14] A. Baraean, M. Kassas, M. S. Alam, and M. A. Abido, "Hybrid neural network and adaptive terminal sliding mode MPPT controller for partially shaded standalone PV systems," *Arab. J. Sci. Eng.*, vol. 48, no. 11, pp. 15527–15539, 2023.

[15] R. G. Mohamed, H. M. Hasanien, and M. A. Ebrahim, "Global MPPT controllers for enhancing dynamic performance of photovoltaic systems under partial shading condition," e-Prime – Adv. Electr. Eng., Electron. Energy, vol. 9, Art. no. 100638, 2024.

[16] N. Benabdallah, B. Belkacem, A. Tahri, H. Benbouhenni, R. Bouddou, S. Heroual, S. Zaidi, Z. M. S. Elbarbary, and S. A. Mohammed, "Enhancing MPPT optimization with hybrid predictive control and adaptive P&O for better efficiency and power quality in PV systems," *Sci. Rep.*, vol. 15, Art. no. 24559, 2025, doi: 10.1038/s41598-025-10335-0.

[17] J. Prakash and S. K. Sahoo, "Design of soft switching interleaved boost converter for photovoltaic application," *Res. J. Appl. Sci. Eng. Technol.*, vol. 9, no. 4, pp. 296–308, 2015, doi: 10.19026/rjaset.9.1408.

[18] Y. Amara, "A comparison analysis between a fixed and multi-step size MPPTs for PV system under variable irradiance and real solar curve," *Int. J. Eng. Manag. Res.*, vol. 12, no. 3, pp. 136–144, Jun. 2022, doi: 10.31033/ijemr.12.3.20.

[19] B. Ge, F. Z. Peng, and Y. Li, "Multilevel converter/inverter topologies and applications," in *Power Electronics for Renewable Energy Systems, Transportation, and Industrial Applications*, H. Abu-Rub, M. Malinowski, and K. Al-Haddad, Eds. Hoboken, NJ, USA: Wiley–IEEE Press, 2014, ch. 18, pp. 422–462.

[20] R. Niu, H. Zhang, and J. Song, "Model predictive control of DC–DC boost converter based on generalized proportional integral observer," *Energies*, vol. 16, Art. no. 1245, 2023, doi: 10.3390/en16031245.

[21] V. Paduani, L. Song, B. Xu, and N. Lu, "Maximum power reference tracking algorithm for power curtailment of photovoltaic systems," *Proc. IEEE Power & Energy Soc. Gen. Meet.*, pp. –, 2021, doi: 10.1109/PESGM46819.2021.9638127.

[22] H. Li, Q. Liu, Z. Zhang, X. Jiang, G.Cao and Y. Zhang, "A voltage overshoot design method for DC–DC converter based on state overshoot concept," in Proc. IECON 2021 – 47th Annual Conf. IEEE Ind. Electron. Soc., Toronto, ON, Canada, 2021, pp. 1–6, doi: 10.1109/IECON48115.2021.9589276.

[23] C. İncebay, " Fotovoltaik Sistem İçin Bulanık Mantık Destekli Adaptif PID Tabanlı Maksimum Güç Noktası İzleyici Tasarımı", M.S. thesis, Inst. of Graduate Studies, Dept. of Electrical and Electronics Eng., Tokat Gaziosmanpasa Univ., Tokat, Turkey, 2025.

[24] M. G. Villalva, J. R. Gazoli, and E. R. Filho, "Comprehensive approach to modeling and simulation of photovoltaic arrays," *IEEE Trans. Power Electron.*, vol. 24, no. 5, pp. 1198–1208, May 2009.

[25] R. Singh, S. Kumar, A. Gehlot, and R. Pachauri, "An imperative role of sun trackers in photovoltaic technology: A review," *Renew. Sustain. Energy Rev.*, vol. 82, pp. 3263–3278, Aug. 2018, doi: 10.1016/j.rser.2017.10.018.

[26] R. Menak, Design and modeling of a dual-axis solar tracking system, M.S. thesis, Dept. of Electrical and Electronics Eng., Siirt Univ., Siirt, Turkey, 2018.

[27] S. Büyükkelek, *Development of a model-based hybrid MPPT method for photovoltaic applications*, M.S. thesis, Konya Technical Univ., Konya, Turkey, 2024.

[28] N. Çoruh, T. Erfidan, and S. Ürgün, "Design and implementation of DC-DC boost converter," *Elektrik Mühendisleri Odası (EMO)*, presented paper, Turkey, [Online]. Available: https://www.emo.org.tr/ekler/22f3e199a63dcb5_ek.pdf

[29] A. Nonaka, "Boost converter inductor sizing effects on the performance of MPPT algorithms," M.S. thesis, Dept. of Electrical Engineering, California Polytechnic State Univ., San Luis Obispo, CA, USA, Aug. 2020.

[30] M. Yılmaz, " Güneş Enerji Sistemleri İçin Yeni Bir Hibrit MPPT Yönteminin Geliştirilmesi ve Gerçek Zamanlı Uygulaması", *Ph.D. dissertation*, Dept. of Electrical and Electronics Engineering, Graduate School of Natural Sciences, Atatürk University, Erzurum, Türkiye, 2024.

[31] T. Şahin, " Fotovoltaik Sistemlerde Kısmi Gölgelenme Durumları İçin Hibrit Maksimum Güç Noktası İzleyicisi Tasarımı", *M.Sc. thesis*, Dept. of Electrical and Electronics Engineering, Institute of Science, Sakarya University, Sakarya, Türkiye, Jan. 2025.

[32] R. B. Bollipo, S. Mikkili, and P. K. Bonthagorla, "Hybrid, optimal, intelligent and classical PV MPPT techniques: A review," *CSEE Journal of Power and Energy Systems*, vol. 7, no. 1, pp. 9–33, 2020, doi: 10.17775/CSEEJPES.2020.00440.

[33] A. Harrag and S. Messalti, "Variable step size modified P&O MPPT algorithm using GA-based hybrid offline/online PID controller," *Renewable and Sustainable Energy Reviews*, vol. 49, pp. 1247–1260, 2015.

[34] H. H. Mousa, A. R. Youssef, and E. E. Mohamed, "State of the art perturb and observe MPPT algorithms based wind energy conversion systems: A technology review," *International Journal of Electrical Power & Energy Systems*, vol. 126, p. 106598, 2021.

[35] K. H. Hussein, I. Muta, T. Hoshino, and M. Osakada, "Maximum photovoltaic power tracking: an algorithm for rapidly changing atmospheric conditions," *IEE Proceedings - Generation, Transmission and Distribution*, vol. 142, no. 1, pp. 59–64, 1995.

[36] J. Kennedy and R. Eberhart, "Particle swarm optimization," *Proc. IEEE Int. Conf. Neural Networks (ICNN'95)*, Perth, Australia, vol. 4, pp. 1942–1948, 1995, doi: 10.1109/ICNN.1995.488968.

[37] A. L. M. Leopoldino, C. M. Freitas, and L. F. C. Monteiro, "Analysis of the Hybrid PSO-InC MPPT for Different Partial Shading Conditions," Advances in Electrical and Computer Engineering, vol. 22, no. 2, pp. 29-36, 2022, doi: 10.4316/AECE.2022.02004.

[38] E. W. Mukti, A. Risdiyanto, A. A. Kristi, and R. Darussalam, "Particle Swarm Optimization (PSO) based Photovoltaic MPPT Algorithm under Partial Shading Condition," Jurnal Elektronika dan Telekomunikasi (JET), vol. 23, no. 2, pp. 99-107, Dec. 2023, doi: 10.55981/jet.552.

[39] K. L. Lian, J. H. Jhang, and I. S. Tian, "A Maximum Power Point Tracking Method Based on Perturb-and-Observe Combined With Particle Swarm Optimization," *IEEE Journal of Photovoltaics*, vol. 4, no. 2, pp. 626-633, March 2014, doi: 10.1109/JPHOTOV.2013.2297513.

[40] A. Chaturvedi, *"Performance Evaluation of MPPT Algorithms on Solar PV System for Asynchronous Loads,"* M.Tech thesis, Dept. of Electrical and Electronics Engineering, University of Petroleum and Energy Studies, Dehradun, India, 2022.

[41] C. L. S. Srinivas and S. E., "A Maximum Power Point Tracking Technique Based on Ripple Correlation Control for Single Phase Photovoltaic System with Fuzzy Logic Controller," *Energy Procedia*, vol. 90, pp. 69–77, 2016.

[42] S. Manna, A. K. Akella, and D. K. Singh, "Novel Lyapunov-based rapid and ripple-free MPPT using a robust model reference adaptive controller for solar PV system," *Protection and Control of Modern Power Systems*, vol. 8, no. 13, 2023.